DFT Study on the Propagation Kinetics of Free-Radical Polymerization of R-Substituted Acrylates

ARTICLE *in* MACROMOLECULES · MARCH 2009

Impact Factor: 5.8 · DOI: 10.1021/ma802875z

DFT Study on the Propagation Kinetics of Free-Radical Polymerization of α-Substituted Acrylates

İ. Değirmenci and V. Aviyente*

Chemistry Department, Boğazici University, 34342, Bebek, Istanbul, Turkey

V. Van Speybroeck and M. Waroquier

Center for Molecular Modeling, Ghent University, Proeftuinstraat 86, 9000 Gent, Belgium

Received December 29, 2008; Revised Manuscript Received March 2, 2009

ABSTRACT: The kinetics of the free-radical propagation of methyl acrylate (MA), methyl methacrylate (MMA), ethyl α-fluoroacrylate (EFA), ethyl α-chloroacrylate (ECA), ethyl α-cyanoacrylate (ECNA), and methyl α-hydroxymethacrylate (MHMA) have been calculated using quantum chemical tools. Various DFT functionals such as BMK, BB1K, MPW1B95, MPW1K, and MPWB1K were used to model the relative propagation kinetics of the monomers. Among the methodologies used, MPWB1K/6-311+G(3df,2p)//B3LYP/6-31+G(d) was found to yield the best qualitative agreement with experiment. We explored chain length effects by examining addition reactions of monomeric, dimeric, trimeric, and tetrameric radicals to the monomers. We have also modeled the tacticity of the widely used monomers MA and MMA by considering all of the alternatives of attack of the radical in the 3D space around the monomer. This study has qualitatively confirmed the experimental syndiotactic/isotactic ratio of 66/3 for MMA. Finally, the kinetics of the initiation to polymerization for MA and MMA is also successfully reproduced.

Introduction

Radical polymerization processes are complex processes involving many different reactions. Even in simple homopolymerization, initiation, propagation, and termination steps occur; also, the propagating species may undergo chain transfer processes. The rates of these individual steps govern the overall rate of polymerization. In the literature, widely deviating values have been reported for rate coefficients. Pulsed laser polymerization size-exclusion chromatography (PLP-SEC) techniques have been used for propagation rate constants, k_p, measurements.[1,2] The ability to measure the rates of the individual reactions and to study the reaction mechanisms and their structure−reactivity relationships will lead to the development of better kinetic models and better methods for controlling free-radical polymerization (FRP).[3] From an experimental point of view, the relation between the polymer chain length and the observed propagation rates for the bulk FRP of styrene and MMA has been studied by several groups. Olaj et al. observed a slight decrease in k_p in terms of chain length.[4] Willemse showed that k_p is dependent on only the chain length in the oligomeric range,[5] but this point of view has been rejected again by Olaj et al.[6] The latter claim that a long-range chain length dependence of k_p extends over several hundreds of propagation steps. This fact is interpreted in terms of a decrease in the monomer concentration at the site of propagation caused by the segments already added to the growing chain.[4−6] The use of quantum chemistry to calculate rate coefficients for FRP is expected to complement the experimental findings. Heuts et al. have used the transition-state theory to predict accurate absolute rate coefficients in FRP.[7,8] They have suggested the low frequency torsional mode of the forming bond to be treated as a 1D hindered internal rotor.[9] This model has been adopted by Van Speybroeck et al., who compared the calculated rate coefficients for radical addition reactions with a 2D method.[10,11] The latter have shown that the chain length dependence of the calculated propagation rate coefficient in polyethylene converges by the hexyl radical. Huang et al. have calculated the propagation rate coefficients of acrylonitrile and methacrylonitrile using a "heavy" unimer.[12] In this study, the frequency factor of methacrylonitrile has shown excellent agreement with experiment, but the barrier was highly dependent on the level of theory. Coote et al. have developed a systematic methodology for calculating accurate propagation rate coefficients in the FRP of acrylonitrile and vinyl chloride.[13] For small- to medium-sized polymer systems, the G3(MP2)-RAD methodology gave accurate results. For larger systems, G3(MP2)-RAD barriers have been approximated via an ONIOM-based approach in which the core is studied at the G3(MP2)-RAD level, and the substituent effects are modeled with the ROMP2/6-311+G(3df,2p) methodology.[3] Yu et al. have applied a similar systematic methodology to methyl acrylate (MA) and methyl methacrylate (MMA) monomers. B3LYP with five different basis sets (6-31G(d),6-31G(d,p),6-311G(d,p),6-311+G(d,p),and6-311G(3df,2p)), MPWB1K/6-31G(d,p), and B1B95/6-31G(d,p) were used to investigate the influence of the method and the basis set on the propagation kinetics of this class of monomers.[14] Recently, Değirmenci et al. have studied the reactivity of a series of acrylates and methacrylates to understand the effect of the pendant group size, the polarity of a pendant group, and the nature of the pendant group (linear vs cyclic) on their polymerizability.[15] As we mentioned in our previous study on the FRP of acrylates and methacrylates, direct comparison between experiment and theory is not trivial, and we tend to focus on relative trends rather than on the reproduction of absolute experimental values.[15]

In this study, we model the propagation kinetics of six monomers displayed in Figure 1. The experimental propagation rate constants are known and are tabulated in Table 1. While the relative propagation rates of the monomers are discussed, various DFT functionals have been tested and the chain length dependence of the polymerization kinetics has been investigated. The tacticity of the widely used monomers MA and MMA has also been modeled. Comparison of the computational findings with experimental results is expected to shed light on the FRP mechanism of this class of monomers.

* Corresponding author. E-mail: aviye@boun.edu.tr.

10.1021/ma802875z CCC: $40.75
Published on Web 03/26/2009

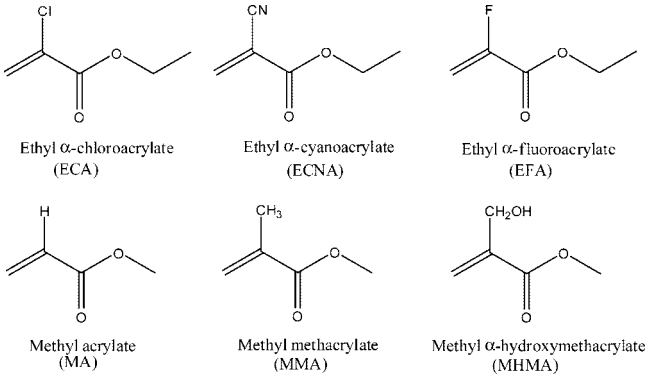

Figure 1. α-Substituted acrylates considered in this study.

Table 1. Experimental Propagation Rate Constants (k_p) of the α-Substituted Acrylates Considered in This Study at 30 °C

	name	k_p (m^3/mol·s)	relative (k_p)
M1	ethyl α-chloroacrylate (ECA)	1.66[c]	4.56
M2	ethyl α-cyanoacrylate (ECNA)	1.62[c]	4.46
M3	ethyl α-fluoroacrylate (EFA)	1.12[c]	3.08
M4	methyl acrylate (MA)	1.48×10^{1}[a,b]	40.67
M5	methyl methacrylate (MMA)	$(3.64 \times 10^{-1}) \pm 0.020$[a,b]	1.00
M6	methyl α-hydroxymethacrylate (MHMA)	0.037[d,e]	

[a] Ref 16. [b] Ref 17. [c] Ref 18. [d] Ref 19. [e] This is the rate of polymerization in mol·L^{-1}·s^{-1}.

Methodology

Reaction Mechanism. The FRP is known to start by the generation of free radicals from the nonradicalic species (initiator)

$$I \xrightarrow{k_d} R\cdot \quad \text{(initiation)}$$

The radical R·, taken to be the methyl (CH_3·) radical, adds to the acrylate monomer and forms a backbone with three C atoms. This species then adds to the monomer to generate the propagating polymer chain (propagation reaction).

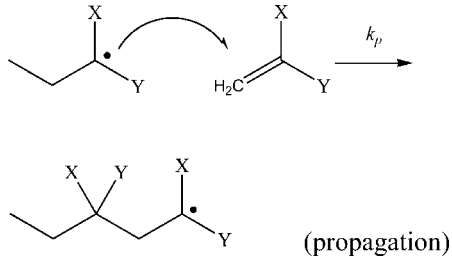

The propagation kinetics of the above-mentioned reaction is modeled in this study. This scheme assumes head-to-tail propagation, which was recently shown to be most favorable.[20]

Computational Procedure. We performed all geometry optimizations by using the Gaussian 03 program package.[21] The B3LYP method is known to yield good ground-state geometries but also to underestimate predictions for reaction barriers and to reproduce weak interaction energies badly.[22] We used the B3LYP/6-31+G(d) methodology for locating the stationary points along the potential energy surface because it is a cost-effective method and was already used to model the free-radical propagation reaction steps.[14,15] Various density functional methods BMK,[23] BB1K,[24,25] MPW1B95,[25] MPW1K,[26] and MPWB1K[25] have been employed for the computation of the energetics starting from the B3LYP/6-31+G(d) optimized structures. It is known that the more exact exchange is taken into account in DFT methods; the larger become reaction barriers resulting from the calculations.[26] The functionals fulfilling these requirements are BMK, MPW1K, and MPWB1K and are expected to yield good results for kinetics and, in particular, higher (and presumably more realistic) barrier heights.[23,25,26] The best agreement with experiment has, in fact, been reproduced with the MPWB1K/6-311+G(3df,2p)//B3LYP/6-31+G(d) methodology.

Scheme 1. Schematic Representation of the Monomers and Their Radicals

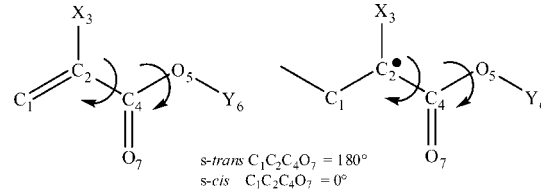

Reaction Kinetics. The conventional transition-state theory (TST) is used to calculate the rate constants. The rate equation of a bimolecular reaction A + B → C is given by[27]

$$k(T) = \frac{k_B T}{h} K_C^{\ddagger}$$

$$K_C^{\ddagger} = \frac{q_{TS}}{q_A q_B} e^{-\Delta E_0 / k_B T}$$

where k_B represents the Boltzmann constant, T is the temperature, h is Planck's constant, ΔE_0 represents the molecular energy difference between the activated complex and the reactants (with inclusion of zero-point vibrational energies), and q_{TS}, q_A, and q_B are the molecular partition functions of the transition state and reactants, respectively.

Results

Geometrical Features of the Monomers and the Radicals. A conformational search for the monomers and the radicals was carried out to find out the most stable structure of these species (Scheme 1). For all of the species, the s-*cis* ($C_1C_2C_4O_7 = 0°$) and s-*trans* ($C_1C_2C_4O_7 = 180°$) conformers have the lowest energies (Figure 2.). All monomers except MMA and MHMA are more stable in their s-*cis* conformations. Note that the s-*trans* conformer of MMA is 0.26 kcal/mol more stable than its s-*cis* conformer, and the barrier between the two conformers is ~5 kcal/mol (Figure 2). The s-*cis* preference of the monomers has been attributed to the stabilizing long-range (C_1)H·····O_7 interactions. The relative energies of the s-*cis*/s-*trans* monomers and syn/anti radicals range from 0.3 to 1.8 kcal/mol (Table 2).

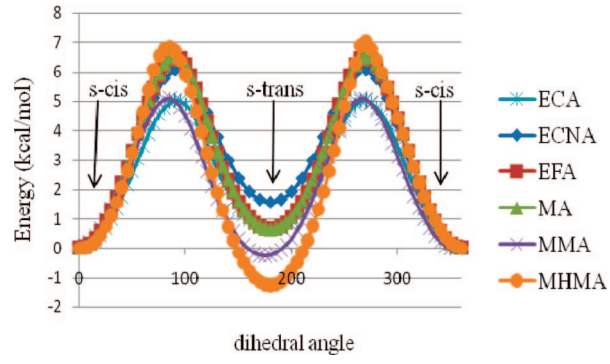

Figure 2. Rotational potential (kcal/mol) as a function of the dihedral angle ($C_1C_2C_4O_7$) for monomers M1−M6.

Table 2. Relative Energies (kcal/mol) of the s-*cis* and s-*trans* Conformers of the Monomers and Their Radicals (B3LYP/6-31+G(d))

	Monomer		Radical	
ECA(s-*cis*)	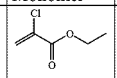	-0.60	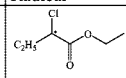	-1.14
ECA(s-*trans*)	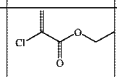	0.00	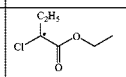	0.00
ECNA (s-*cis*)	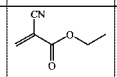	-1.47	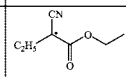	-1.74
ECNA(s-*trans*)	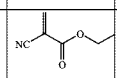	0.00	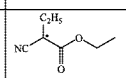	0.00
EFA (s-*cis*)	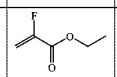	-0.61	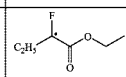	-1.14
EFA(s-*trans*)	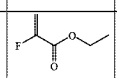	0.00	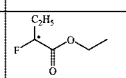	0.00
MA (s-*cis*)	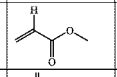	-0.64	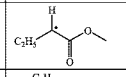	-0.54
MA(s-*trans*)	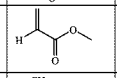	0.00	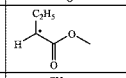	0.00
MMA (s-*cis*)	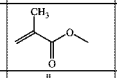	0.00	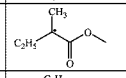	-0.06
MMA(s-*trans*)	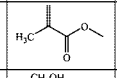	-0.26	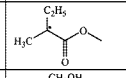	0.00
MHMA(s-*cis*)	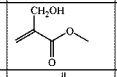	0.00	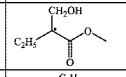	0.00
MHMA(s-*trans*)	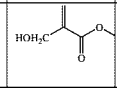	-1.11	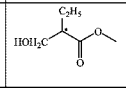	-0.99

To dissect the different stabilizing factors in s-*cis* and s-*trans* conformations, NBO analysis at the B3LYP/6-311+G(3df,2p)//B3LYP/6-31+G(d) level has been carried out for MA and MMA.[28] The hyperconjugative energy of "donor−acceptor" (bond−antibond) interactions in the NBO analysis has been considered to quantify the bond delocalization energy. For MA, the hyperconjugative interaction energy for the *s-cis* conformer is 7.56 kcal/mol higher than that for its *s-trans* conformer. Similarly, for MMA, the *s-cis* conformer is more stabilized (8.82 kcal/mol) than the *s-trans* conformer because of hyperconjugative interactions. The main contribution to the stabilization of the monomer structure comes from antibonding interactions between BD*(2) $C_4 = O_7 \rightarrow$ BD*(2) $C_1 = C_2$. However, in both the s-*cis* and s-*trans* conformers of MA and MMA, the charge separations lead to electrostatic interactions that play a crucial role (Figure 3). A close inspection of the electrostatic attraction forces reveals the fact that in both cases the s-*trans* conformer is favored over the s-*cis* conformer. However, notice also that in the case of s-*trans* MMA the carbonyl oxygen,O_7, is in close proximity to four H atoms, whereas in the case of s-*trans* MA, the carbonyl oxygen interacts with only three H atoms. Therefore, the extra stabilization of the s-*trans* MMA with respect to the s-*cis* MMA can be attributed to the long-range attractive interactions between the carbonyl oxygen and the methyl group. This stabilizing interaction is missing in MA. Overall, even though delocalization stabilizes the s-*cis* conformations of MA and MMA, the electrostatic interactions between the methyl group and the carbonyl oxygen can be considered

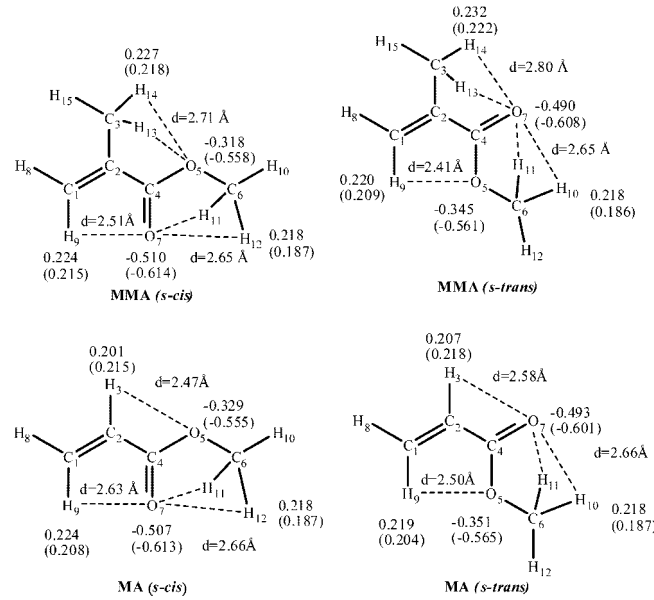

Figure 3. Mulliken and NBO charges (in parentheses) of the most stable s-*cis* and s-*trans* conformers of MMA and MA.

to be the major source stabilizing the s-*trans* conformation of MMA.

Tacticity of MA and MMA. Although various effective methods of stereoregulation have been devised for anionic and coordination polymerizations, only limited successful examples are known for FRP, even though many classes of polymers are industrially produced by radical catalysis.[2,29] Therefore, the stereoregulation of radical polymerization is an especially challenging goal. The tacticity of vinyl polymers often significantly affects the properties of the polymers. However, many industrially important vinyl polymers including poly(methyl methacrylate) (PMMA) and polystyrene (PS) are produced by radical polymerization, which is more versatile and economical compared with other types of polymerizations but is generally poor in stereocontrol. Therefore, the development of stereoregulation methods for radical polymerization can contribute to the industrial production of polymers with improved properties.[2] The control of the stereochemistry in acrylate polymerizations is important because physical properties of acrylate polymers are often significantly influenced by the main-chain tacticity. In a recent experimental study, the syndiotactic/isotactic ratio of MMA has been found to be 66/3.[29] Therefore, in this study, the tacticity of the polymerizing chain has been analyzed prior to the kinetics of propagation. We demonstrate that the growing polymer radical, which is generated from the s-*trans* and s-*cis* conformers of the monomer, produces two different stereoisomers. The transition structures for all of the monomers under investigation have been located by considering the attack of the radical in the form of $CH_3CH_2C\cdot(X)-C(O)-OCH_3$ to the monomer ($H_2C{=}C(X)-C(O)-OCH_3$). As depicted in Scheme 2, there are two approaches of the radical to the monomer leading to distinct transition states, labeled (+) and (−). Attack from the (+) direction yields syndiotactic products, whereas attack from the (−) direction yields isotactic products, emphasizing that the direction of attack ((+) or (−)) specifies the tacticity of the final product. Overall, we have located eight different transition states generated by the attack of the syn and anti conformers of each radical to the s-*cis* and s-*trans* conformers of the monomer. The tacticity of the products as well as the reaction barriers relative to the most favorable transition state are given in Table 3.

A rotational potential energy scan is performed for rotation about the forming bond in the search for each transition state.

Scheme 2. Stereoselective Radical (syn) Addition to MA (MMA) (s-*cis* and s-*trans*)

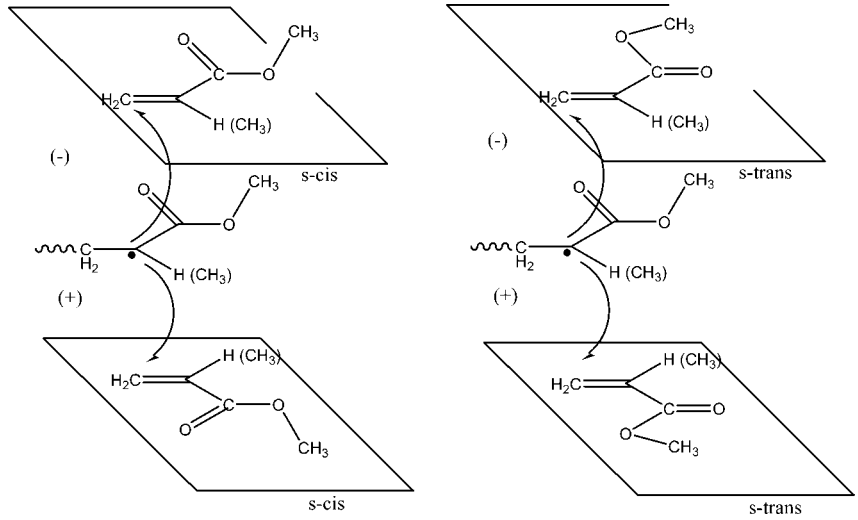

Table 3. Relative Reaction Barriers (B3LYP/6-31+G(d), kcal/mol) for the Transition States Leading to Syndiotactic and Isotactic MA(MMA) Dimeric Chains

R\M	s-*cis*	s-*trans*
syn (+)	syndiotactic	syndiotactic
	0.00(0.00)	1.15(0.69)
syn (−)	isotactic	isotactic
	0.17(0.29)	1.04(0.79)
anti (+)	syndiotactic	syndiotactic
	1.12(0.35)	2.15(0.87)
anti (−)	isotactic	isotactic
	1.07(0.23)	1.91(0.83)

This study reveals that the addition of the *syn*-MA and *syn*-MMA radicals to the s-*cis*-MA and s-*cis*-MMA monomers from the (+) direction yielding a syndiotactic chain is favored over the others (Table 3). Nevertheless, the attack along the reverse side of the monomer (the (−) direction) leading to an isotactic dimeric chain requires slightly more energy, and hence both reactions are competitive with respect to each other. For the syndiotactic polymerization of MA starting from the s-*cis* stereoconformation, two significant minima are found in the rotational potential energy curve: the global minimum is found at torsional angle θ ($C_1C_2C_3C_4$) = 176.83°; the local minimum corresponding to a gauche addition is barely higher (Figure 4). A similar procedure is followed for the isotactic polymerization of MA for which the global minimum along the potential energy surface of the forming bond lies at θ = 49.60°. The local minimum for the transition structure is still the gauche addition (θ = −50.70°) (Figure 4).

Table 3 also reveals that the reaction barriers of the addition reactions belonging to the other stereoisomers besides s-*cis*- are somewhat higher, but conclusive remarks should be handled with care because the change of monomer from MA to MMA reduces the reaction barrier differences within a range of 0.9 kcal/mol. In this study, the propagation kinetics for all of the monomers of interest will be modeled for the attack of the syn radical to the s-*cis* monomer from the (+) direction.

Similarly, for the syndiotactic polymerization of MMA, the global minimum along the potential energy scan around the forming bond lies at torsional angle θ ($C_1C_2C_3C_4$) = 60.13°; the local minimum for the transition structure is the anti addition θ = −170.02°. For the isotactic polymerization of MMA, the global minimum lies at θ = 49.88°. The local minimum for the transition structure is the gauche addition (θ = −71.63°), which corresponds to ∼300° (Figure 5).

A conformer search about the newly formed bond was carried out for the syndiotactic polymers (dimeric chains) for MMA and MA (Figure 6). It is clearly seen that in both cases the growing backbone tends to be in a plane with the carbon atoms of the growing backbone being anti to each other. (Figure 7).

Transition Structures for the Propagation of the Monomers. For all of the monomers except MHMA, the most favorable transition structures correspond to the attack of the radical in a syn conformation to the s-*cis* stereoisomer of the monomer (Figure 8). The s-*trans* conformer of MHMA is favored over its s-*cis* conformer because of the intramolecular hydrogen bonding interactions between the −CH_2OH group and the carbonyl oxygen. The geometries of the transition states are such that the attack of the radical to the monomer is gauche except for MA. The potential energy scans for MMA, ECA, EFA, and ECNA have their minima at approximately similar torsional angles of ∼60°.

The C···C bond distance of the forming bond in the transition states shows a relatively good relationship with the heat of the propagation reaction, $-\Delta H_{rxn}$ (Figure 9). The longer the C−C distance, the more the structure resembles the separated reactants, the closer the transition structure is to the reactants, and finally, the more exothermic the reaction is as expected from Hammond's postulate. The addition of a reactive carbon-centered radical to a molecule with a multiple carbon− carbon bond is generally exothermic because a π bond is replaced by a σ bond.[30] Therefore, and according to Hammond's postulate,[31] the transition state is early; that is, the cleavage of the π bond and the formation of the σ bond are far from being complete in the transition structure.

Propagation Rate Constants of the Various Monomers at Different Levels of Theory. In the preceding subsections, the geometrical features and the tacticity control in the FRP of MA and MMA have been discussed. It has been demonstrated that syndiospecific and isospecific propagations take place with a slight preference for the formation of syndiotactic MA (MMA) dimeric chains. However, the differences in reaction barriers are very low and are not really conclusive because of the rather low level of theory (B3LYP/6-31+G(d)). Nevertheless, this study gives a qualitative overview of the various stereospecific radical polymerization reactions. In what follows, we have attempted to have a deeper understanding of the kinetics of the FRP of the acrylate derivatives with the aim of testing DFT functionals, which would yield propagation rate constants closer to the experimental ones. Table 4 gathers the free-radical propagation rate constants of the various monomers obtained at different levels of theory together with the experimental

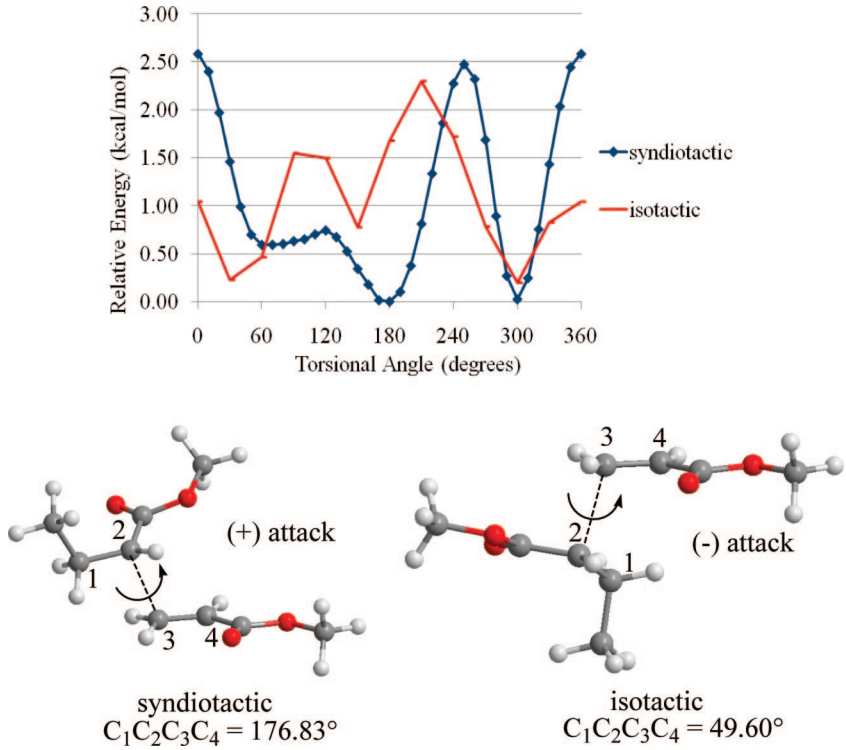

Figure 4. Rotational potential energy scan and transition-state structures for syndiotactic (syn(+)s-*cis*) and isotactic (syn(−)s-*cis*) propagation of MA (B3LYP/6-31+G(d)).

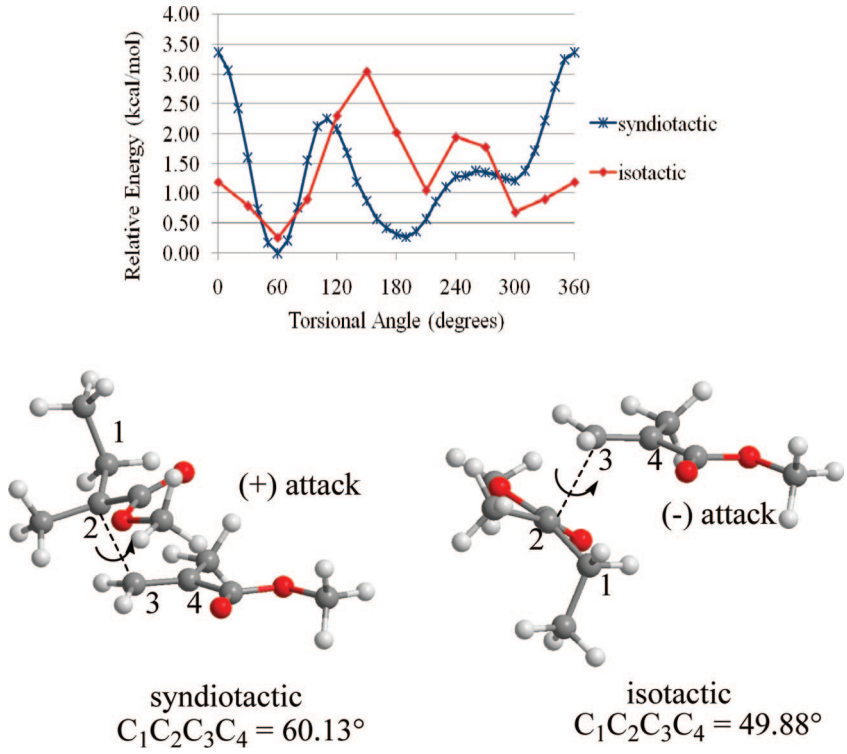

Figure 5. Potential energy scan and transition-state structures for syndiotactic (syn(+)s-*cis*) and isotactic (syn (−)s-*cis*) propagation of MMA (B3LYP/6-31+G(d)).

results. A reliable methodological approach for studying radical propagation reactions is expected to stem from this study. The transition structures for the dimeric syndiotactic chains (syn(+)s-*cis*) are considered in every case. The level of theory (LOT) study showed that the most reliable results are obtained by using MPWB1K and MPW1B95 methods (Figure 10). Nevertheless, the experimental trend is best reproduced with MPWB1K, and the kinetics in this study are evaluated with this method.

Chain Length Dependency. Earlier studies in the literature have clearly shown that the use of too-short chains can incur large errors, and this adds further support to the notion that penultimate unit effects are important in free-radical copolymerization. Coote et al. have shown that for acrylonitrile and vinyl chloride, the minimum-sized chemical model that can reliably mimic the polymerization system is the $n = 1.5$ system (n is an integer that labels the propagation reaction, $n = 1$ for a unimer,

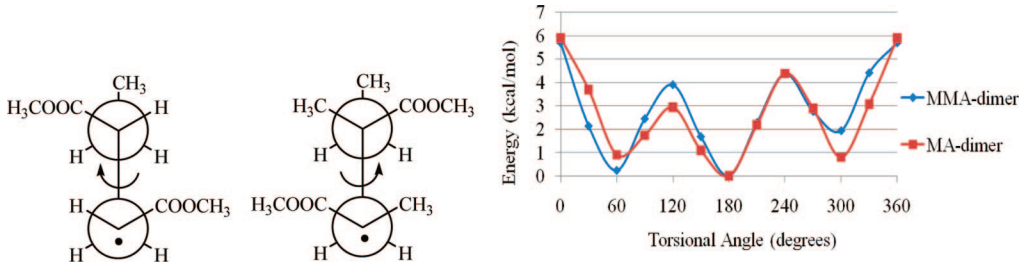

Figure 6. Conformational search for the intermediate products (dimeric chains) of MA and MMA and their Newman projections.

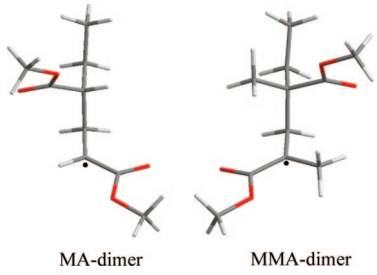

Figure 7. 3D structures for the intermediate products (dimeric chains) of MA and MMA.

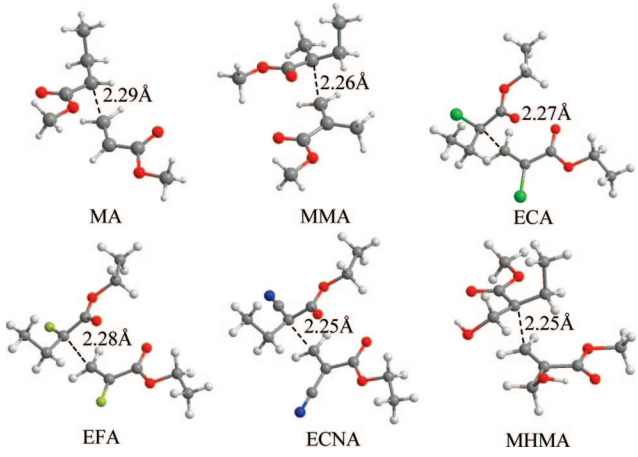

Figure 8. Most stable transition structures for the propagation of the monomers (B3LYP/6-21+G(d)).

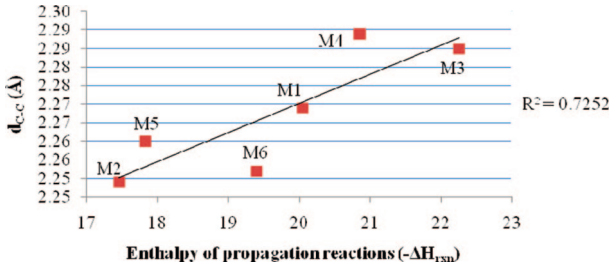

Figure 9. Dependence of the C···C bond distance on the heat of reaction ($-\Delta H_{rxn}$) in the transition states of the dimeric radicals (MPWB1K/6-311+G(3df,2p)//B3LYP/6-31+G(d)).

$n = 2$ for a dimer, etc.). This model has produced excellent relative values of the barriers and frequency factors and has produced absolute values of the rate coefficients that agree to within a factor of 1.6 of their corresponding long chain values. Scheme 3 illustrates how the chain length effect on propagation rate constant is modeled. We used the monomeric radical and the monomer itself to calculate k_{P1}. k_{P2} is calculated by the attack of the generated dimeric radical chain to the monomer. The third and fourth steps are also modeled in the same way. The chain length dependency is illustrated by the attack of the radical in a syn conformation to the s-*cis* stereoisomer of the monomer while the chain grows.

The results in Table 5 and Figure 11 show that the effect of the chain length on the propagation rate constants can amount to a factor of 10. Some rate constants are oscillating, whereas others exhibit a smooth behavior. A real convergence regime is not yet reached at $n = 4$; in general, k_p decreases as the chain gets longer. Among the monomers of interest, MMA propagates the slowest experimentally; this finding is reproduced no matter what the length of the monomer is. In Table 5, the relative rate constants, k_p (in parentheses), show a better agreement with experiment as the chain gets longer. There is one exception, EFA, where the predicted relative trend does not coincide with the experimental findings. The chain length dependence of all of the monomers in this study is expected to converge as n increases, as in previous studies of Van Cauter et al.[11] and Coote et al.[13]

Syndiotactic versus Isotactic Polymerization of MMA. Isobe et al. have shown that the bulk polymerization of MMA gives an isotactic, atactic, and syndiotactic mixture in the ratio of 3/31/66, respectively.[2,29] All of the possible transition-state structures leading to syndiotactic and isotactic MMA dimeric chains have been located to obtain average rate constants in each case (Figure 12). The rate constant for the isotactic transition state is denoted as *ki1* when starting from the s-*cis* monomer; it is denoted as *ki2* when starting from the s-*trans* monomer. Similarly, the rate constants are denoted as *ks1* and *ks2* for the corresponding syndiotactic transition states. The Boltzmann distribution is used to calculate the relative population of the s-*cis* and s-*trans* conformations of the monomer. The overall rate constant is the weight average of the two rate constants. In this way, the average rate constant for the syndiotactic product is $\langle ks \rangle = 2.29 \times 10^{-3}$. (Notice that this value is very close to the rate constant corresponding to the most probable path, 2.63×10^{-3}, reported earlier in Tables 4 and 5). The average rate constant $\langle ki \rangle$ for the isotactic product is 1.01×10^{-3}. Therefore, at the MPWB1K/6-311+G(3df,2p)//B3LYP/6-31+G(d) level, the $\langle ks \rangle/\langle ki \rangle$ ratio is 2.28, which is in qualitative agreement with Isobe's results.[29] Overall, our calculations show the major component of PMMA to be syndiotactic, as experimentally observed. The effect of the media on the kinetics and tacticity of the FRP of MMA has been investigated by Isobe et al., where the syndiotactic specificity of MMA was enhanced by the use of fluoroalcohols, including $(CF_3)_3COH$ as a solvent.[29] Our work in progress includes the FRP of MMA in different media to assess the origin of the stereocontrol in the FRP of MMA and lead experimentalists in their future endeavors.

Initiation versus Propagation Reactions of MA and MMA. Even though MA polymerizes 40 times faster than MMA,[16,17] the rate coefficients for the initiation of these monomers by the addition of 2-cyano-2-propyl radical generated from the decomposition of the commonly employed initiator 2,2′-azoisobutyronitrile (AIBN)) are 4.30 times faster for

Table 4. Propagation Rate Constants (k_p) of the Monomers at Different Levels of Theory in the Temperature Range 250 < T < 350 K[a]

	B3LYP/6-31+G(d)	B3LYP	BMK	MPW1K	BB1K	MPWB1K	MPW1B95	exptl k_p (m^3/mol·s)
ECA	2.45×10^{-4}	6.08×10^{-5}	8.44×10^{-3}	2.02×10^{-3}	2.77×10^{-3}	3.77×10^{-2}	6.09×10^{-2}	1.66[d]
ECNA	1.10×10^{-4}	4.13×10^{-6}	3.58×10^{-3}	1.38×10^{-3}	1.60×10^{-3}	2.14×10^{-2}	3.81×10^{-2}	1.62[d]
EFA	3.46×10^{-3}	8.68×10^{-4}	8.01×10^{-3}	9.13×10^{-3}	4.67×10^{-3}	5.24×10^{-2}	1.01×10^{-1}	1.12[d]
MA	1.29×10^{-2}	4.24×10^{-3}	2.31×10^{-2}	4.47×10^{-2}	1.75×10^{-2}	1.11×10^{-1}	2.36×10^{-1}	1.48×10^{1}[b,c]
MMA	7.43×10^{-6}	1.70×10^{-6}	2.84×10^{-4}	7.55×10^{-5}	1.72×10^{-4}	2.63×10^{-3}	3.91×10^{-3}	3.64×10^{-1}[b,c]
MHMA	3.37×10^{-4}		1.34×10^{-2}	2.56×10^{-3}	1.09×10^{-2}	1.63×10^{-1}	2.62×10^{-1}	

[a] Geometries are calculated at the B3LYP/6-31+G(d) level, and kinetics are determined with different DFT methods at the 6-311+G(3df,2p) level unless otherwise stated. [b] Ref 16. [c] Ref 17. [d] Ref 18.

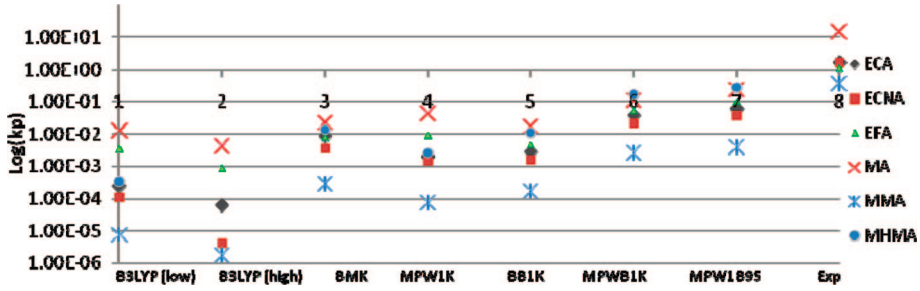

Figure 10. Log(k_p) versus different methodologies.

Scheme 3. Propagation Steps of the Growing Chain[a]

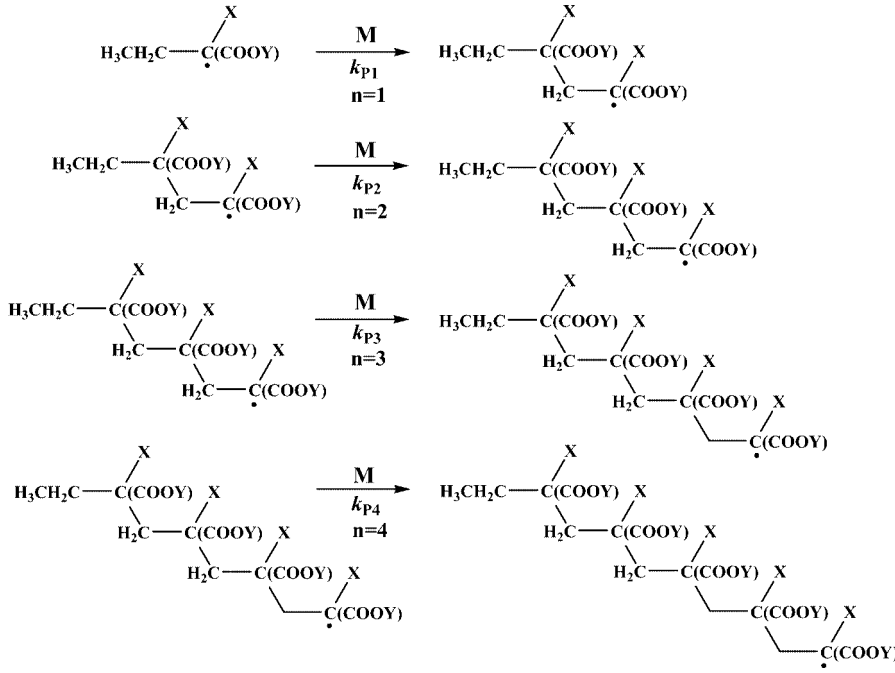

[a] X = −H, −CH_3, −F, −Cl, −CN, −CH_2OH; Y = −CH_3 for MA, MMA, MHMA, and Y = −CH_2CH_3 for EFA, ECA, ECNA.

Table 5. Chain Length Dependency of the Propagation Rate Constants, k_p (m^3/mol·s), with the Transition Structures for the Dimeric Syndiotactic Chains (syn(+)s-*cis*) Considered in Every Case (MPWB1K/6-311+G(3df,2p)//B3LYP/6-31+G(d), 250 < T < 350 K)[a]

	$n = 1$	$n = 2$	$n = 3$	$n = 4$	exptl k_p
ECA	3.77×10^{-2} (14.34)	4.36×10^{-3} (8.17)	3.49×10^{-3} (2.97)	5.33×10^{-3} (6.11)	1.66 (4.56)
ECNA	2.14×10^{-2} (8.14)	6.85×10^{-3} (12.85)	1.76×10^{-2} (14.98)	5.16×10^{-3} (5.92)	1.62 (4.46)
EFA	5.24×10^{-2} (19.93)	1.82×10^{-2} (34.19)	3.56×10^{-2} (30.24)	2.59×10^{-2} (29.65)	1.12 (3.08)
MA	1.11×10^{-1} (42.16)	1.09×10^{-1} (205.12)	8.72×10^{-2} (74.05)	6.33×10^{-2} (72.64)	1.48×10^{1} (40.67)
MMA	2.63×10^{-3} (1.00)	5.34×10^{-4} (1.00)	1.18×10^{-3} (1.00)	8.72×10^{-4} (1.00)	3.64×10^{-1} (1.00)
MHMA	1.63×10^{-1} (61.96)	1.53×10^{-1} (287.48)	1.51×10^{-1} (128.65)	1.71×10^{-1} (195.53)	

[a] Values in parentheses are rate constants relative to MMA.

MMA.[32] This intriguing behavior of these two commercially widely used monomers has been clarified in what follows.

The MPWB1K/6-311+G(3df,2p)//B3LYP/6-31+G(d) methodology at 315.15 K has been used to evaluate the average initiation rate constant <k_{ini}> for MA to be 1.95×10^{-4} and the one for MMA to be 1.02×10^{-3}. Also note that <k_{ini}> in Table 6 refers to the average rate constant for the initiation of both MA and MMA relative to both the s-*cis* and s-*trans* conformations of the monomers. Figure 13 illustrates the addition of 2-cyano-2-propyl radical (i.e., the radical generated from the decomposition of the commonly employed initiator 2,2′-azoisobutyronitrile (AIBN)) to MA and MMA at 315.15 K. Our

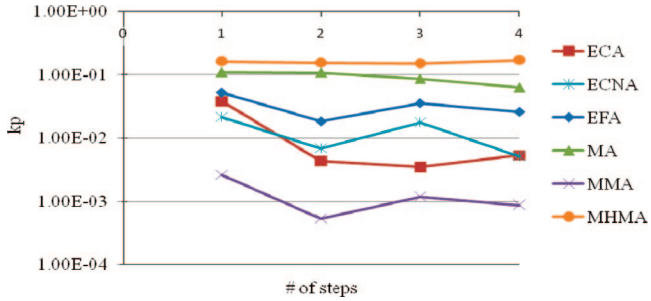

Figure 11. Propagation rate constant, k_p (m^3/mol·s), as a function of the number of units in growing chain at MPWB1K/6-311+G(3df,2p)//B3LYP/6-31+G(d).

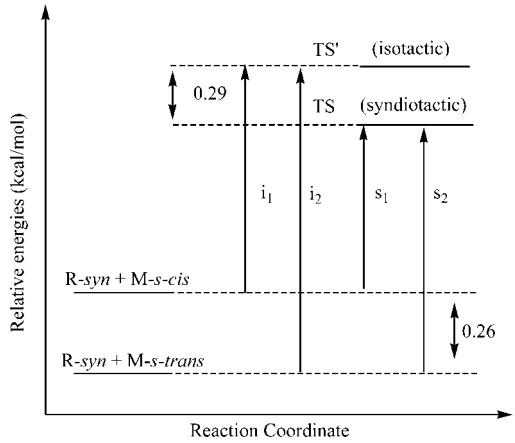

Figure 12. Most probable pathways for syndiotactic and isotactic MMA.

Table 6. Kinetic Parameters for the Initiation and the Propagation Steps of MA and MMA (MPWB1K/6-311+G(3df,2p)//B3LYP/6-31+G(d), (250 < *T* < 350 K))[a]

	initiation			propagation	
monomer	*A* (m^3/mol·s)	E_a (kcal/mol)	$\langle k_{ini} \rangle$ (m^3/mol·s)	*A* (m^3/mol·s)	E_a (kcal/mol)
MA	2.02×10^2	8.42	1.95×10^{-4}	3.28×10^3	5.80
MMA	5.64×10^2	8.49	1.02×10^{-3}	2.95×10^1	6.09

[a] *A* and E_a refer to s-*cis* MA and s-*trans* MMA, and $\langle k_{ini} \rangle$ is the average rate constant for initiation for both conformations in both cases.

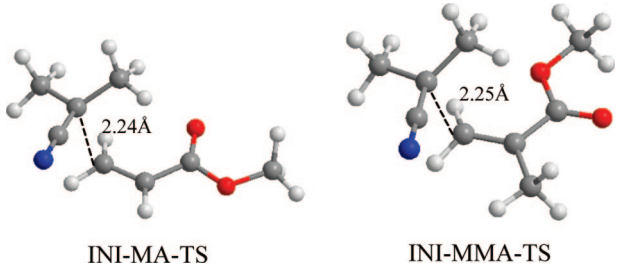

Figure 13. Initiation transition-state geometries for MA and MMA (B3LYP/6-31+G(d)).

results indicate the initiation of MMA to be 5.20 times faster than the initiation of MA. This ratio is in good qualitative agreement with the experimental results by Heuts et al., who have determined this ratio to be 4.30 on the basis of the rate coefficients for the addition of 2-cyano-isopropyl radical to MA (0.37 m^3/mol·s) and to MMA (1.59 m^3/mol·s).[32]

Furthermore, Heuts et al. have found the initiation step of MA to have a higher energy barrier (2.7 kcal/mol) than the propagation step. This increase in the activation energy is claimed to be due to the stability of the conjugated cyano radical.

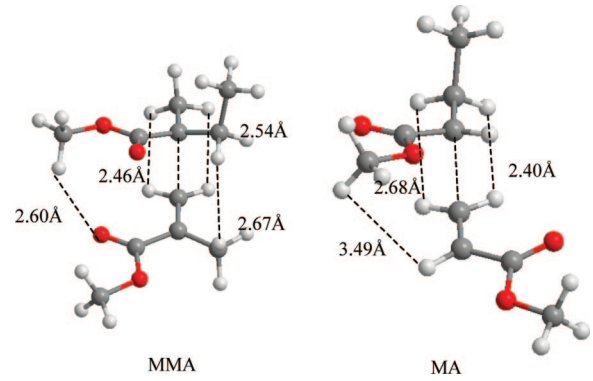

Figure 14. Representation of intramolecular interactions in the transition states of MMA and MA.

Our computational results (Table 6) are in agreement with the experimental prediction: in both cases, the activation barrier for initiation is higher than that for propagation by ~2.5 kcal/mol. Experimentally, the accelerated initiation of MMA as compared to MA has been attributed to the magnitude of the preexponential factor, *A*.[32] Our calculations confirm the experimental behavior; the preexponential factor *A* is almost three times larger for MMA than for MA, presumably because tertiary radicals (MMA-R) are expected to be less disordered than secondary radicals (MA-R).

The propagation reaction of MA is faster than that of MMA because of the higher preexponential entropy factor (the transition state is more disordered) and also because of the lower activation barrier. In the case of MMA, steric repulsions between the hydrogen atoms of the methyl groups repel each other (Figure 14). Not only steric repulsions but also electronic properties of the transition states have an important effect on the activation barriers (Table 6). The dipole moment of the most stable transition state for MMA-anti (μ = 2.036 D) is higher than that for the most stable transition state of MA-gauche (μ = 1.871 D).

Conclusions

In this study, the propagation reaction in the FRP of MA, MMA, EFA, ECA, ECNA, and MHMA has been modeled with DFT. Among the various functionals (BMK, BB1K, MPW1B95, MPW1K, MPWB1K) tested, the MPWB1K/6-311+G(3df.2p)//B3LYP/6-31+G(d) methodology is found to give the best agreement with experiment. The chain length dependency has been examined by the addition of monomeric, dimeric, trimeric, and tetrameric radicals to the monomers. The syndiotactic versus isotactic preference of MMA has been reproduced; finally, the initiation versus propagation reactions of MA and MMA have been rationalized. Overall, this study has demonstrated the fact that computational chemistry offers a viable alternative to experiment: relative propagation rate coefficients as well as tacticity can be predicted prior to FRP.

Acknowledgment. The computational resources used in this work were provided by the TUBITAK ULAKBIM High-Performance Computing Center, the Bogazici University Research Foundation (projects 03M501 and 05HB501), Tubitak (project 105T223), and the Center of Molecular Modeling, University of Ghent. V.V.S. and M.W. acknowledge the Fund for Scientific Research Flanders (FWO) and the Fund for Scientific Research of the Ghent University for financial support. We acknowledge the sixth framework project COSBIOM (FP6-2004-ACC-SSA-2.517991) for funding the travel and lodging expenses of İ.D.,V.A., and V.V.S. in UG and BU.

References and Notes

(1) (a) Heuts, J. P. A.; Russell, G. T.; Simith, G. B.; Van Herk, A. M. *Macromol. Symp.* **2007**, *248*, 12–22. (b) Buback, M.; Gilbert, R. G.; Hutchinson, R. A.; Klumperman, B.; Kuchta, F. D.; Manders, B. G.; O'Driscoll, K. F.; Russell, G. T.; Schweer, J. *Macromol. Chem. Phys.* **1995**, *196*, 3267–3280. (c) Beuermann, S.; Buback, M.; Davis, T. P.; Gilbert, R. G.; Hutchinson, R. A.; Olaj, O. F.; Russell, G. T.; Schweer, J.; van Herk, A. M. *Macromol. Chem. Phys.* **1997**, *198*, 1545–1560.

(2) (a) Isobe, Y.; Yamada, K.; Nakano, T.; Okamoto, Y. *Macromolecules* **1999**, *32*, 5979–5981. (b) Nakano, T.; Okamoto, Y. In *Controlled Radical Polymerization*; Matyjazsewski, K., Ed.; ACS Symposium Series 685;American Chemical Society: Washington, DC, 1998; pp 451−462. (c) Pino, P.; Suter, U. W. *Polymer* **1976**, *17*, 977–995. (d) Hatada, K.; Kitayama, T.; Ute, K. *Prog. Polym. Sci.* **1988**, *13*, 189–276. (e) Yuki, H.; Hatada, K. *Adv. Polym. Sci.* **1979**, *31*, 1–45.

(3) Coote, M. *Aust. J. Chem.* **2004**, *57*, 1125–1132.

(4) Olaj, O. F.; Vana, P.; Zoder, M.; Kornherr, A.; Zifferer, G. *Macromol. Rapid Commun.* **2000**, *21*, 913–920.

(5) Willemse, R. X. E.; Staal, B. B. P.; van Herk, A. M.; Pierik, S. C. J.; Klumperman, B. *Macromolecules* **2003**, *36*, 9797–9803.

(6) Olaj, O. F.; Zoder, M.; Vana, P.; Kornherr, A.; Schnöll-Bitai, I.; Zifferer, G. *Macromolecules* **2005**, *38*, 1944–1948.

(7) Heuts, J. P. A.; Gilbert, R. G.; Radom, L. *Macromolecules* **1995**, *28*, 8771–8781.

(8) Heuts, J. P. A.; Gilbert, R. G.; Radom, L. *J. Phys. Chem.* **1996**, *100*, 18997–19006.

(9) (a) Vansteenkiste, P.; Van Neck, D.; Van Speybroeck, V.; Waroquier, M. *J. Chem. Phys.* **2006**, *124*, 044314. (b) Van Speybroeck, V.; Van Cauter, K.; Coussens, B.; Waroquier, M. *ChemPhysChem* **2005**, *6*, 180–189. (c) Van Speybroeck, V.; Van Neck, D.; Waroquier, M.; Wauters, S.; Saeys, M.; Marin, G. B. *J. Phys. Chem. A.* **2000**, *104*, 10939–10950.

(10) Van Speybroeck, V.; Van Neck, D.; Waroquier, M. *J. Phys. Chem. A* **2002**, *106*, 8945–8950.

(11) Van Cauter, K.; Van Speybroeck, V.; Vansteenkiste, P.; Reyniers, M. F.; Waroquier, M. *ChemPhysChem* **2006**, *7*, 131–140.

(12) Huang, D. M.; Monteiro, M. J.; Gilbert, R. G. *Macromolecules* **1998**, *31*, 5175–5187.

(13) Izgorodina, E. I.; Coote, M. *Chem. Phys.* **2006**, *324*, 96–110.

(14) Yu, X.; Pfaendtner, J.; Broadbelt, L. J. *J. Phys. Chem. A* **2008**, *112*, 6772–6782.

(15) Değirmenci, I.; Avcı, D.; Aviyente, V.; Van Cauter, K.; Van Speybroeck, V.; Waroquier, M. *Macromolecules* **2007**, *40*, 9590–9602.

(16) Buback, M.; Kurz, C. H.; Schmaltz, C. J. *Macromol. Chem. Phys.* **1998**, *199*, 1721–1727.

(17) (a) Beuermann, S.; Buback, M.; Thomas, P. D.; Gilbert, R. G.; Hutchinson, R. H.; Olaj, O. F.; Russell, G. T.; Schweerh, J.; Van Herk, A. M. *Macromol. Chem. Phys.* **1997**, *198*, 1545–1560. (b) Zammit, M. D.; Coote, M.; Davis, T. P.; Willett, G. *Macromolecules* **1998**, *31*, 955–963. (c) Bauerman, S.; Buback, M. *Prog. Polym. Sci.* **2002**, *27*, 191–254. (d) Van Herk, A. M. *Macromol. Theory Simul.* **2000**, *9*, 433–441.

(18) Yamada, B.; Kontani, T.; Yoshioka, M.; Otsu, T. *J. Polym. Sci., Polym. Chem. Ed.* **1984**, *22*, 2381–2393.

(19) Avcı, D.; Mathias, L. J.; Thigpen, K. *J. Polym. Sci., Part A: Polym. Chem.* **1996**, *34*, 3191–3201.

(20) Van Cauter, K.; Van Speybroeck, V.; Waroquier, M. *ChemPhysChem* **2007**, *8*, 541–552.

(21) Frisch, M. J.; Trucks, G. W.; Schlegel, H. B.; Scuseria, G. E.; Robb, M. A.; Cheeseman, J. R.; Montgomery, Jr., J. A.; Vreven, T.; Kudin, K. N.; Burant, J. C.; Millam, J. M.; Iyengar, S. S.; Tomasi, J.; Barone, V.; Mennucci, B.; Cossi, M.; Scalmani, G.; Rega, N.; Petersson, G. A.; Nakatsuji, H.; Hada, M.; Ehara, M.; Toyota, K.; Fukuda, R.; Hasegawa, J.; Ishida, M.; Nakajima, T.; Honda, Y.; Kitao, O.; Nakai, H.; Klene, M.; Li, X.; Knox, J. E.; Hratchian, H. P.; Cross, J. B.; Bakken, V.; Adamo, C.; Jaramillo, J.; Gomperts, R.; Stratmann, R. E.; Yazyev, O.; Austin, A. J.; Cammi, R.; Pomelli, C.; Ochterski, J. W.; Ayala, P. Y.; Morokuma, K.; Voth, G. A.; Salvador, P.; Dannenberg, J. J.; Zakrzewski, V. G.; Dapprich, S.; Daniels, A. D.; Strain, M. C.; Farkas, O.; Malick, D. K.; Rabuck, A. D.; Raghavachari, K.; Foresman, J. B.; Ortiz, J. V.; Cui, Q.; Baboul, A. G.; Clifford, S.; Cioslowski, J.; Stefanov, B. B.; Liu, G.; Liashenko, A.; Piskorz, P.; Komaromi, I.; Martin, R. L.; Fox, D. J.; Keith, T.; Al-Laham, M. A.; Peng, C. Y.; Nanayakkara, A.; Challacombe, M.; Gill, P. M. W.; Johnson, B.; Chen, W.; Wong, M. W.; Gonzalez, C.; Pople, J. A.; *Gaussian 03*, revision D.01; Gaussian, Inc.: Wallingford CT, 2004.

(22) Smith, D. M.; Nicolaides, A.; Golding, B. T.; Radom, L. *J. Am. Chem. Soc.* **1998**, *120*, 10223–10233.

(23) Boese, A. D.; Martin, J. M. L. *J. Chem. Phys.* **2004**, *121*, 3405–3416.

(24) (a) Zhao, Y.; Lynch, B. J.; Truhlar, D. G. *J. Phys. Chem. A* **2004**, *108*, 2715–2719. (b) Zhao, Y.; González-García, N.; Truhlar, D. G. *J. Phys. Chem. A* **2005**, *109*, 2012–2018. (c) Sousa, S. S.; Fernandes, A. P.; Ramos, M. J. *J. Phys Chem A* **2007**, *111*, 10439–10452.

(25) Zhao, Y.; Truhlar, D. G. *J. Phys. Chem. A* **2004**, *108*, 6908–6918.

(26) Lynch, B. J.; Fast, P. L; Harris, M.; Truhlar, D. G. *J. Phys. Chem. A* **2000**, *104*, 4811–4815.

(27) McQuarrie, D. A.; Simon, J. D. *Physical Chemistry: A Molecular Approach*; University Science Books: Sausalito, CA, 1997.

(28) (a) Reed, A. E.; Weinstock, R. B.; Weinhold, F. *J. Chem. Phys.* **1985**, *83*, 735–746. (b) Foster, P.; Weinhold, F. *J. Am. Chem. Soc.* **1980**, *102*, 7211–7218. (c) Reed, A.; Weinhold, E. F. *J. Chem. Phys.* **1983**, *78*, 4066–4073. (d) Reed, A. E.; Weinhold, F. *J. Chem. Phys.* **1985**, *83*, 1736–1740. (e) Reed, A. E.; Curtiss, L. A.; Weinhold, F. *Chem. Rev.* **1988**, *88*, 899–926.

(29) Isobe, Y.; Yamada, K.; Nakano, T.; Okamoto, Y. *J. Polym. Sci., Part A: Polym. Chem.* **2000**, *38*, 4693–4703.

(30) Fischer, H.; Radom, L. *Angew. Chem., Int. Ed.* **2001**, *40*, 1340–1371.

(31) Hammond, G. S. *J. Am. Chem. Soc.* **1955**, *77*, 334–338.

(32) Heuts, J. P. A.; Russell, G. T. *Eur. Polym. J.* **2006**, *42*, 3–20.

MA802875Z